ADVANCED OPTICAL MATERIALS

Supporting Information

for *Adv. Optical Mater.*, DOI 10.1002/adom.202300267

A Novel Multi-Functional Thiophene-Based Organic Cation as Passivation, Crystalline Orientation, and Organic Spacer Agent for Low-Dimensional 3D/1D Perovskite Solar Cells

*Ali Semerci, Ali Buyruk, Saim Emin, Rik Hooijer, Daniela Kovacheva, Peter Mayer, Manuel A. Reus, Dominic Blätte, Marcella Günther, Nicolai F. Hartmann, Soroush Lotfi, Jan P. Hofmann, Peter Müller-Buschbaum, Thomas Bein and Tayebeh Ameri**

Supporting Information

A Novel Multi-Functional Thiophene-Based Organic Cation as the Passivation, Crystalline Orientation, and Organic Spacer Agent for Low-Dimensional 3D/1D Perovskite Solar Cells

Ali Semerci[1,†], Ali Buyruk[1,†], Saim Emin[2], Rik Hooijer[1], Daniela Kovacheva[3], Peter Mayer[1], Manuel A. Reus[4], Dominic Blätte[1], Marcella Günther[1], Nicolai F. Hartmann[5], Soroush Lotfi [6], Jan P. Hofmann[6], Peter Müller-Buschbaum[4,7], Thomas Bein[1], Tayebeh Ameri[1,8]*

[1] Department of Chemistry and Center for NanoScience (CeNS), Ludwig-Maximilians-Universität München (LMU), Butenandtstrasse 5-13 (E), 81377 Munich, Germany

[2] Materials Research Laboratory, University of Nova Gorica, Vipavska 13c, 5270 Ajdovščina, Slovenia.

[3] Institute of General and Inorganic Chemistry, Bulgarian Academy of Sciences, Sofia 1113, Bulgaria

[4] TUM School of Natural Sciences, Department of Physics, Chair for Functional Materials, Technical University of Munich, James-Franck-Str. 1 85748 Garching, Germany.

[5] Attocube systems AG, Nanoscale Analytics, neaspec, Eglfinger Weg 2, 85540 Haar, Germany

[6] Surface Science Laboratory, Department of Materials and Earth Sciences, Technical University of Darmstadt, Otto-Berndt-Strasse 3, 64287 Darmstadt, Germany

[7] Heinz Maier-Leibnitz-Zentrum (MLZ), Technical University of Munich, Lichtenbergstr. 1, 85748 Garching, Germany

[8] Institute for Materials and Processes, Chemical Engineering, University of Edinburgh, Sanderson Building, Robert Stevenson Road, EH9 3FB Edinburgh, Scotland, U.K.

*Email: tayebeh.ameri@ed.ac.uk

1. Materials and reagents

The SnO_2 colloid precursor was purchased from Alfa Aesar (tin (IV) oxide, 15% in H_2O colloidal dispersion). Before spin-coating as an ETL, the SnO_2 nanoparticles were diluted with deionized water (DI) to 2.67 wt.%. The organic spacer precursor 2-(2-thienyl) pyridine (98%) unprotonated form), as well as PbI_2 and methyl ammonium iodide (MAI), were purchased from TCI. MACI, bathocuproin (BCP), solvents (dimethyl sulfoxide (DMSO), N,N-dimethylformamide (DMF), etc.) and freshly delivered hydroiodic acid (HI ~57 wt.%) were purchased from Sigma-Aldrich. The 2,2′,7,7′-tetrakis-(N,N-di-4-methoxyphenyl amino)-9,9′-spirobifluorene (Spiro-OMeTAD) used as an HTL material was purchased from Borun Chem. The (PEDOT:PSS) aqueous solution and phenyl-C61-butyric acid methyl ester ($PC_{61}BM$) were purchased from Ossila.

2. Solar cell fabrication:

2a. Fabrication of bulk-passivated 3D MAPI solar cell

ITO substrates (3 cm x 3 cm) were first etched using 3 M Hydrochloric acid (HCl) and Zn powder and later rinsed with deionized water. This was followed by sonication of the substrates in 2% detergent (Hellmanex™ III) aqueous solution, DI water, ethanol, and isopropanol for 15 min each, respectively. Afterwards the substrates were dried in nitrogen flow and treated with nitrogen plasma for 15 min. PEDOT: PSS was spin-coated onto pre-cleaned Indium Tin Oxide (ITO) substrates at 2500 rpm for 40 s and annealed at 140 ℃ for 20 min in air. After this process, the substrates were transferred into a glovebox for device fabrication.

Bulk-passivated 3D perovskite precursor solution was prepared from the stoichiometric ratio of PbI_2, MAI and ThPyI at molar ratio 3:2:2, respectively, in a 1 ml DMF: DMSO (8:1 volume ratio) mixture. For the devices where MACI was used as an additive for preferential crystal orientation, the amount of MACl was adjusted to MACl/MAI 0.5 wt.%. The prepared solution was stirred for 12 h at 70 ℃ . The prepared bulk-passivated 3D perovskite solution was spin coated onto ITO/PEDOT:PSS substrate at 6000 rpm for 40 s. Toluene (350 µl) was dropped onto the perovskite film during the last 15 s of the spin-coating process, followed by heat treatment at 100 ℃ for 15 min. $PC_{61}BM$ (20 mg/mL in chlorobenzene (CB) and BCP (0.6 mg/mL in 2-propanol (IPA) were spin-coated subsequently onto the perovskite active layer at 1000 rpm for 30 s, respectively. In the last step, a 100 nm thick silver electrode was thermally evaporated under vacuum ($1x10^{-6}$ Pa). The active area was fixed to 0.0831 cm^2 using a metal mask. 3D MAPI control devices with and without MACI were fabricated using similar steps as given above but without using ThPyI in the precursor solutions.

2b. Solar cell fabrication with surface-passivated 3D/1D perovskite

FTO substrates (3 cm x 3 cm) were first etched using 3 M HCl and Zn powder and later rinsed with deionized water. This was followed by sonication of the substrates in 2% detergent (Hellmanex™ III) solution, DI water, ethanol, and isopropanol for 15 min each, respectively. Afterwards the substrates were dried in nitrogen flow and treated with nitrogen plasma for 15 min. A diluted SnO_2 nanoparticle solution (2.67 wt% in water) was spin-coated onto the FTO substrate in air at 4000 r.p.m. for 35 s, and then annealed

in air at 150 ^{o}C for 30 min. Before the perovskite coating, the SnO_2 coated substrates were cleaned once again using the UV-O_3 environment for 10 min. Using the one-step "anti-solvent" method, the precursors of the perovskite – PbI_2 (1.68 M, 5% excess), MAI (1.60 M), and DMSO (1.60 M) in 1 mL DMF were deposited on top of the SnO_2 layer at 1000 rpm for 10 s, followed by fast spinning at 3500 rpm for 20 s. Ethyl acetate as an anti-solvent was dropped onto the perovskite film during the last 10 s while spinning. The sample was then annealed at 130 ^{o}C for 10 min. For the surface treatment, the 2-(thiophen-2-yl) pyridin-1-ium iodide salt in isopropanol solution (3.9 mg/ml) was spin-coated onto the perovskite films at 1000 r.p.m for 30 s followed by 5000 r.p.m for 5 s. This was followed by heat treatment of the latter substrate at 100 ^{o}C for 10 min. The hole transport material (HTM) was deposited by spin-coating (3000 rpm for 30 s) a solution containing 72.3 mg spiro-OMeTAD, 35 µl bis(trifluoromethane) sulfonimide lithium salt (LiTFSI) stock solution (270 mg LiTFSI in 1 ml acetonitrile), 30 µl 4-*tert*-butylpyridine and 1 ml chlorobenzene. Finally, a 70 nm thin film of Au was thermally evaporated under high vacuum on top of the HTM layer.

3. General characterization techniques:

UV–vis absorption (UV-vis)*:* were recorded using a Perkin Elmer Lambda 1050 spectrometer with an integrating sphere. Time-resolved photoluminescence

Photoluminescence (PL): spectroscopy was performed with a Picoquant Fluotime 300 spectrofluorometer using an excitation wavelength of 375 nm. Current-voltage (*J-V*) characteristics were measured under ambient conditions using a Newport OrielSol 2A solar simulator (AM 1.5G - 100 mW cm^{-2}) and a Keithley 2400 source meter.

The solar simulator: was calibrated with a Fraunhofer ISE certified silicon cell (KG5-filtered). The active area of the solar cells was defined by a square metal aperture mask with an area equal to 0.0831 cm^2. *J-V* curves were recorded by scanning the input bias from -0.1 V to 1.2 V (forward scan) at a scan rate of 0.1 V/s after the devices had been at 1.2 V for 5 s under illumination. For the light intensity-dependent *J-V*-measurements, a white light LED was used as a light source. The LED intensity was adjusted with a Keithley 2200-20-5 Power Supply. A highly linear photodiode was used to control the light intensity over a range of 0.1 – 1.2 suns. *J-V*-curves were measured with a Keithley 2401 source meter.

External Quantum Efficiency (EQE): To obtain the EQE spectra, the PV cells were illuminated with a chopped light (tungsten lamp) and the beam was passed through a monochromator. Further, the light beam was split to illuminate the sample as well as a reference silicon photodetector (Hamamatsu S2281-01) at the

same time. The resulting wavelength-dependent current response of both devices was recorded simultaneously by two lock-in amplifiers (Signal Recovery 7265, Stanford Research Systems 830) at a chopping frequency of 14 Hz. The incident illumination power, determined via the reference photodetector, was used to calculate the EQE response of the perovskite solar cell.

X-Ray Diffraction (XRD): (XRD) measurements were performed with a Bruker D8 Discover X-ray diffractometer operating at 40 kV and 30 mA. The diffracted X-ray beam was passed through a Ni filter. The Cu Kα1 radiation (λ = 1.5406 Å) and a position-sensitive LynxEye detector were used. ***Powder X-Ray Diffraction (P-XRD)***: P-XRD measurements were carried out on a STOE STADI P diffractometer in Debye–Scherrer geometry, operating at 40 kV and 40 mA, using monochromated (Ge(111) single crystal monochromator) Cu-$K_{\alpha 1}$ radiation (λ = 1.5406 Å) and a DECTRIS MYTHEN 1K detector.

Grazing-incidence wide-angle X-ray scattering (GIWAXS): GIWAXS data measurements were performed on an Anton-Paar Saxspoint 2.0 with a Primux 100 microfocus source with Cu-$K_{\alpha 1}$ radiation (λ = 1.5406 Å) and a Dectris Eiger R 1M 2D Detector.

Scanning Electron Microscopy (SEM): For SEM, an FEI Helios Nanolab G3 UC DualBeam scanning electron microscope (SEM) equipped with an Oxford Aztec Advanced X-Max 80 EDX detector was used. SEM images were recorded at an acceleration voltage of 2 kV. Top view images were recorded using both a backscattered electron detector and a secondary electron through-the-lens detector.

HR-TEM studies**:** Transmission electron microscopy (TEM) studies were carried out with a JEOL 2100F instrument operating at 200 kV. MAPI perovskite thin films (without MACI) were used as source material. Sample preparations were achieved by removing perovskite from the substrate and transferring it on the surface of a lacey coated copper TEM grid.

Single-Crystal X-Ray Diffraction (SC-XRD)**:** The frames were integrated with the Bruker SAINT software package.[1] Data were corrected for absorption effects using the Multi-Scan method (SADABS).[2]. The structure was solved and refined using the Bruker SHELXTL Software Package.[3] All hydrogen atoms have been calculated in ideal geometry riding on their parent atoms. The structure has been refined as a 2-component inversion twin. The domain volume ratio refined to 0.87/0.13. The disorder of the organic cation has been described by a split model. The ratio of site occupation factors of the two disordered parts refined to 0.58/0.42. All atoms of the organic cation have been refined isotropically. Atoms of the main part have been used as geometrical model for the minor part (SAME instruction in SHELX). The SIMU restraint has been

applied for disordered atoms with a distance of 0.8 A or closer. The figures have been drawn at the 25% ellipsoid probability level.[4] In the case of disorder the less-occupied parts have been neglected for the figures.

Crystallographic data have been deposited with the Cambridge Crystallographic Data Centre, CCDC, 12 Union Road, Cambridge CB21EZ, UK. Copies of the data can be obtained free of charge on quoting the depository numbers CCDC-2237540 (https://www.ccdc.cam.ac.uk/structures/).

Nano-FTIR: For nano-FTIR measurements, a commercially available near-field microscope (neaSNOM, Neaspec) was used. For this technique, based on scattering-type scanning optical near-field microscopy (s-SNOM), a sharp, metal-coated AFM tip was illuminated by a broadband IR source. The light backscattered from the oscillating metallic tip was analyzed with an asymmetric Fourier transform spectrometer, which was based on a Michelson interferometer.[4] This allowed for the simultaneous recording of optical amplitude and phase of the backscattered light. To suppress the background light the tip was oscillated harmonically with a small tapping amplitude A and frequency Ω (here A = 65 nm, Ω = 247 kHz) and the detector signal was demodulated at higher harmonics $n\Omega$ of this frequency. For $n \geq 2$ the background is completely suppressed, delivering local near-field amplitude and phase spectra. To eliminate the microscope response function, the spectra were normalized to the spectra obtained from a spectrally flat reference (Si substrate). This resulted in local reflectivity and absorption spectra of the investigated materials. The latter was used for chemical identification according to standard FTIR databases.[5]

To record the nano-FTIR data, silicon wafer (2.5 cm X 2.5 cm) substrates were used. The substrates were sonicated in 2% detergent solution, DI water, ethanol, and isopropanol for 15 min each, respectively. Subsequently, dried substrates were further cleaned via ultraviolet ozone treatment for 15 min before the perovskite coating. The architecture of the thin film follows the order: silicon wafer/$MAPbI_3$/ w/-, w/o the 2-(thiophen-2-yl)pyridin-1-ium iodide salt. Neat perovskite and surface treated perovskite films were fabricated using the same method employed for solar cell fabrication.

Space-Charge Limited Current (SCLC): To evaluate the surface passivation effects on trap-density via the space-charge limited current (SCLC) method, electron-only devices were prepared with the device configuration of ITO/SnO_2/$MAPbI_3$ w or wo ThPyI /PCBM/Au. For bulk-passivated 3D MAPI, the electron-only device configuration is ITO/SnO_2/ Perovskite with MACl w or wo ThPyI /PCBM/BCP/Ag.

Ultraviolet Photoelectron Spectroscopy (UPS). Photoelectron spectroscopy was performed with a PHI 5000 VersaProbe at the Clustertool at InnovationLab GmbH in Heidelberg. The samples were introduced from the glovebox with exposures to air <1 min. UPS was carried out with a He-discharge lamp using the He-I emission with an energy of 21.22 eV. Pass energies of 2.95, and 0.59 eV were used for UPS valence band and UPS secondary electron cut-offs, respectively. For the measurements of the secondary electron cut-off, a bias of −5 V was applied. The take-off angle for all measurements was 90°. The Fermi level of clean silver (Ar sputtered) was used to calibrate the UPS data.

4. Syntheses:

4a. Synthesis of 2-(thiophen-2-yl)pyridin-1-ium iodide salt

The organic spacer precursor (2g, 98% purity,12.16 mmol) – 2-(2-thienyl)pyridine (unprotonated form) – was dissolved in 20 ml IPA. After cooling down to 0 °C in an ice bath, subsequently hydriodic acid ~57 wt.% (1.93 ml, 14.59 mmol) was dropped into the solution. After stirring at 0 °C for 2 h, a yellowish precipitate was observed and then collected by filtration. Collected solids were washed with diethyl ether for three times, dried under vacuum at 50 °C for 24 h to afford the yellowish solid product (3.24 g 92 % yield). ^{1}H NMR (400 MHz, DMSO-d_6) δ 8.62 (ddd, *J* = 5.3, 1.7, 1.0 Hz, 1H), 8.14 – 8.03 (m, 2H), 7.92 (dd, *J* = 3.7, 1.2 Hz, 1H), 7.80 (dd, *J* = 5.0, 1.2 Hz, 1H), 7.50 (ddd, *J* = 6.9, 5.2, 1.7 Hz, 1H), 7.24 (dd, *J* = 5.0, 3.7 Hz, 1H), 7.13 (s, 1H). ^{13}C NMR (101 MHz, DMSO) δ 149.47, 146.65, 140.68, 140.29, 130.38, 128.85, 127.59, 123.21, 120.79. HRMS (ESI, m/z): calculated for $C_9H_8NS^+$ 162.04; found 162.03733 $[M+H]^+$.

4b. Synthesis of single crystals

PbI_2 (0.3 M) and 2-(2-thienyl)pyridine, unprotonated form) (0.3 M) were mixed in a round bottom flask in fresh hydriodic acid ~57 wt.% (20 mL) and stirred at room temperature for 10 minutes. Subsequently, the resulting mixture was heated up to 140 °C and stirred at this temperature for 1 h. After stirring for 1 h, the transparent yellow solution was slowly cooled down to room temperature. During the cooling, at about 110 °C, yellow needle-shape crystals were observed in the solution. The needle-shaped crystals were collected by filtration to remove unreacted PbI_2, which is soluble in the reaction mixture, and subsequently washed several times with diethyl ether. Finally, they were dried at 60 °C in air for 24 h.

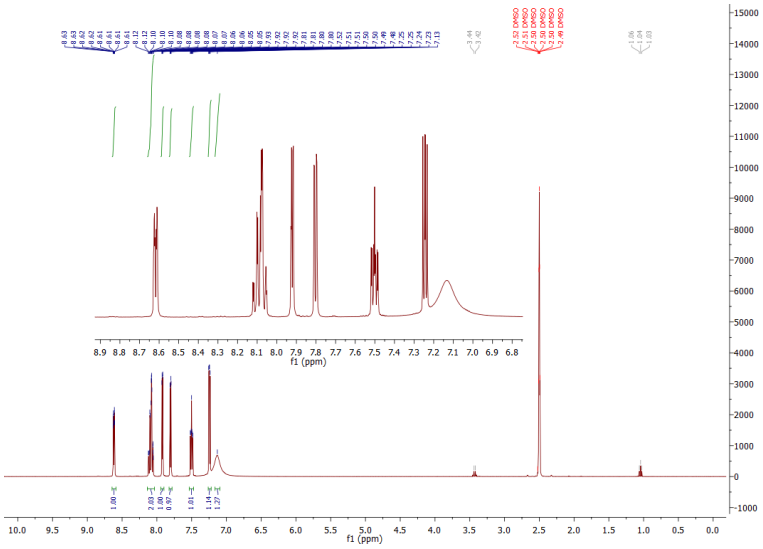

Figure S1a. ^{1}H-NMR spectra of ThPyI organic spacer

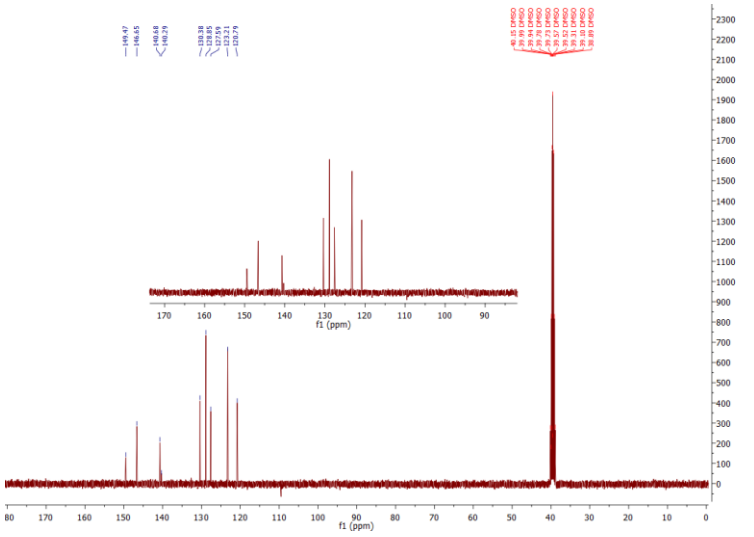

Figure S1b. ^{13}C-NMR spectra of ThPyI organic spacer

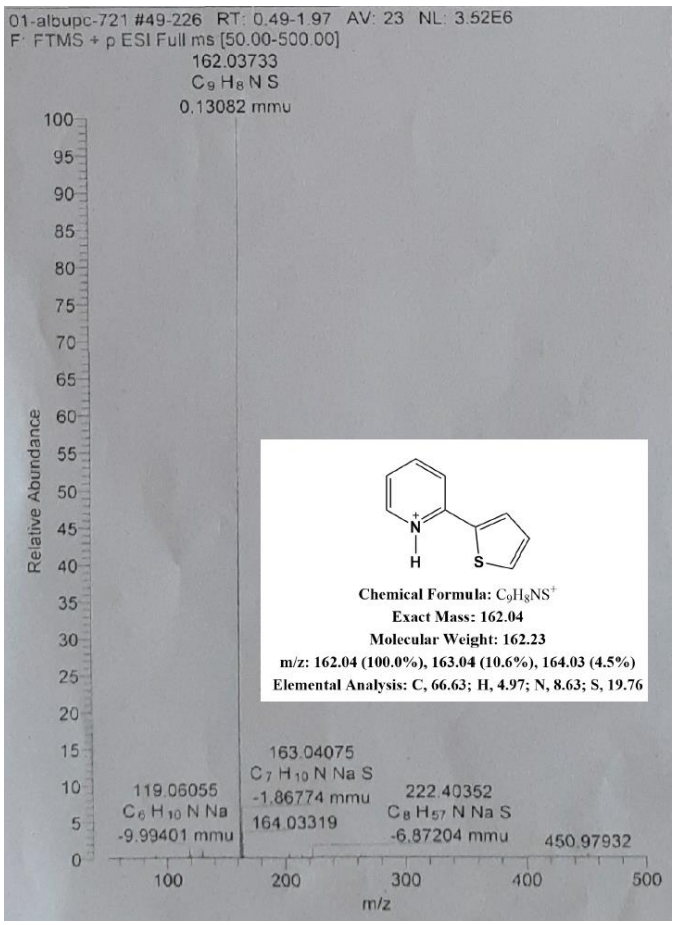

Figure S1c. Mass spectrum of ThPyI organic spacer with a distinctive *m/z* peak at 162.037.

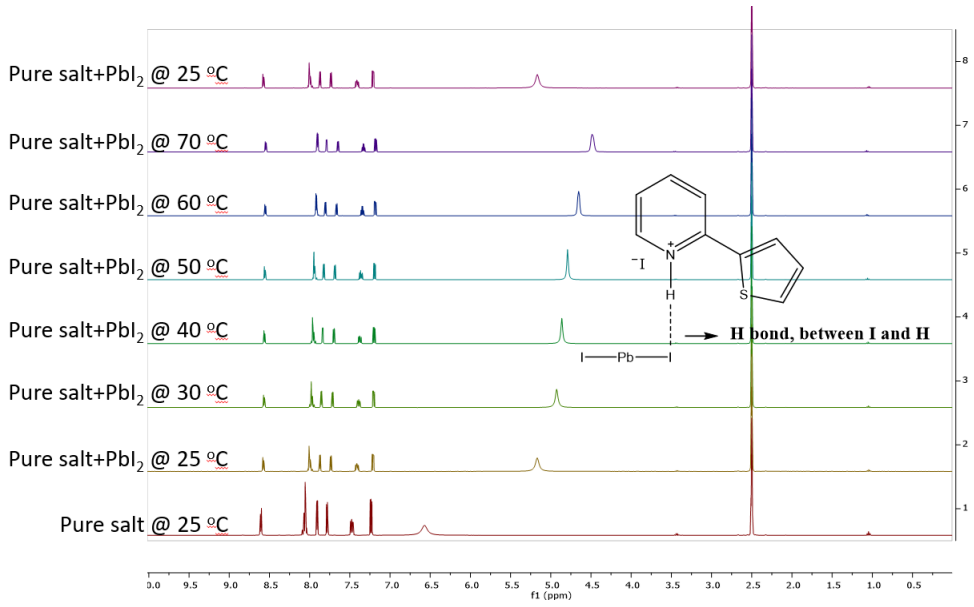

Figure S1d. ^{1}H-NMR spectra of PbI_2 + ThPyI mixture at different temperatures

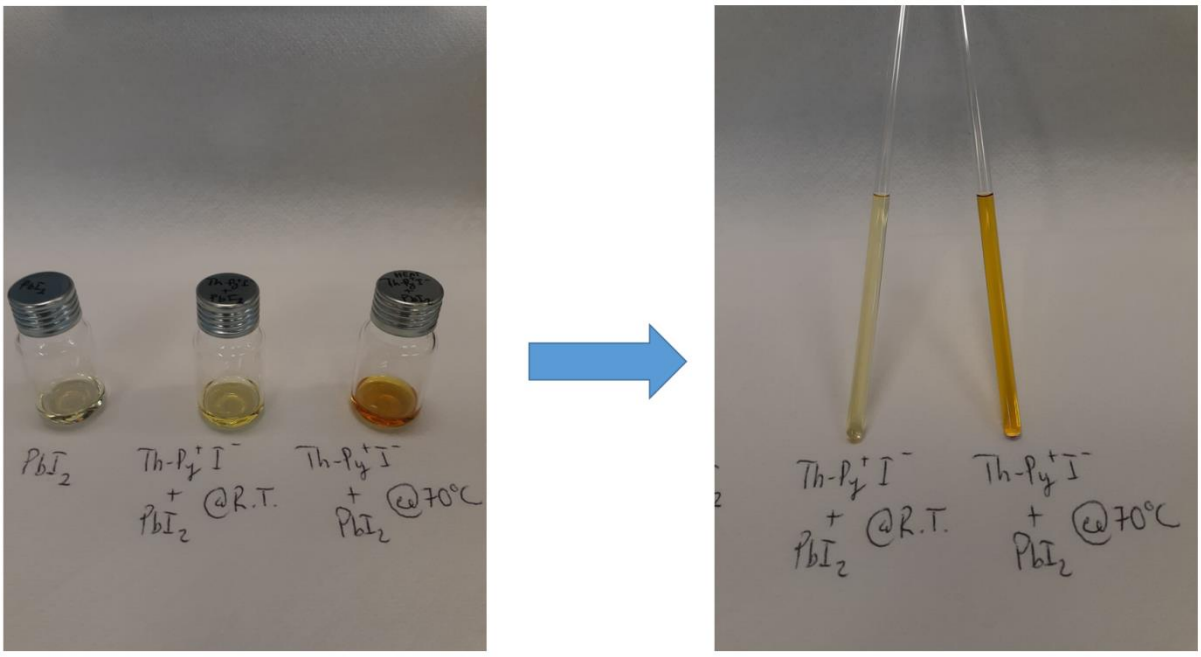

Figure S1e. Photos of the PbI_2 + ThPyI mixture after heating at different temperatures

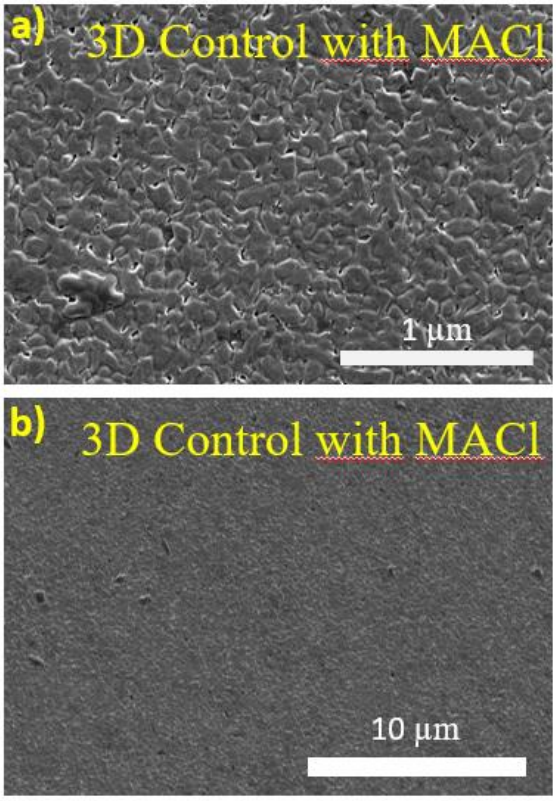

Figure S2. SEM images of a, b) 3D control with MACl

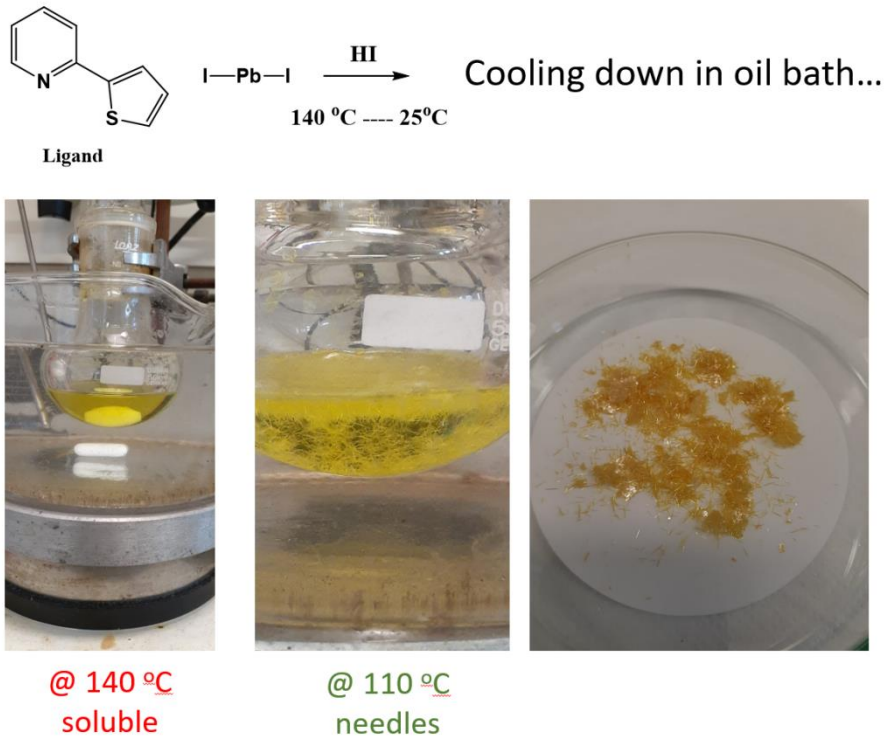

Figure S3. Photos of the 1D single crystals forming during the synthesis.

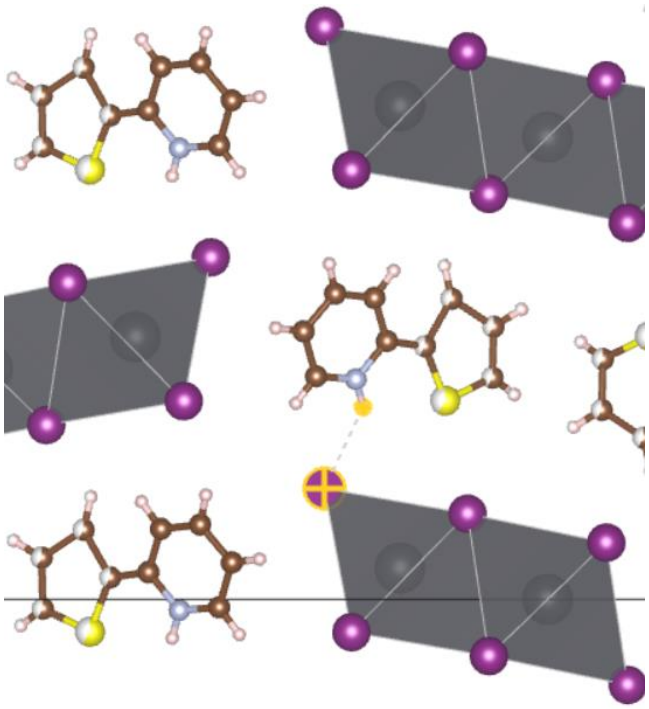

Figure S4. N^{+}-H···I-PbI_5 hydrogen-bonding interaction (l(H1-I4) = **2.8118(2) Å**

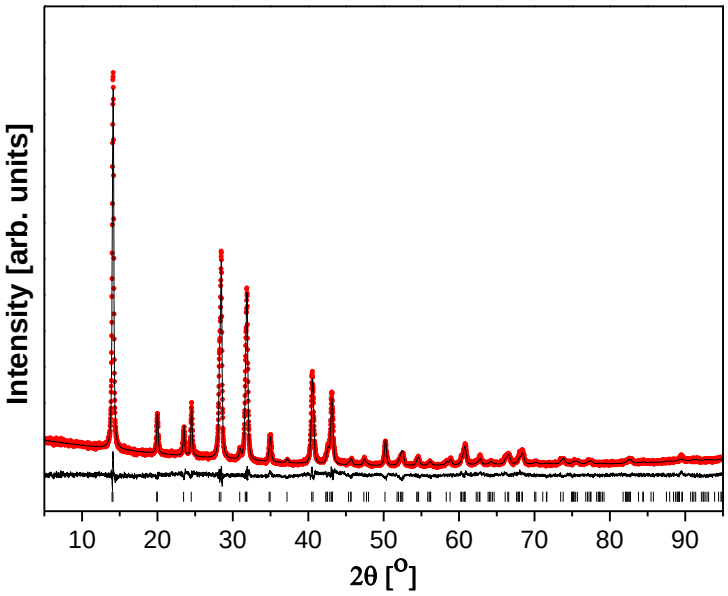

Figure S5. Rietveld plot for the 3D-control sample. Red dots – Y_{obs}, black line – Y_{calc}, line below – Difference, Vertical bars – Bragg positions.

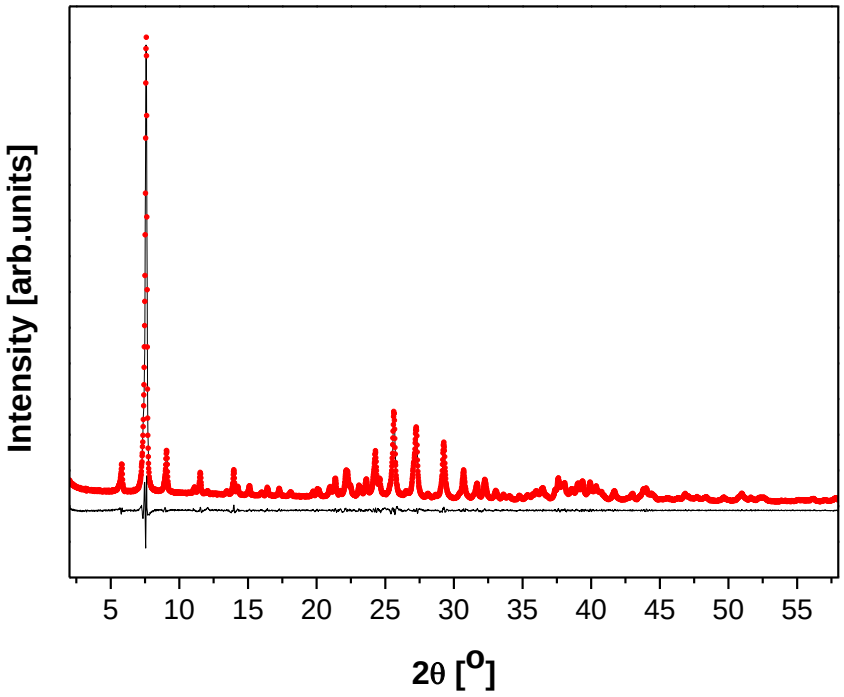

Figure S6. Le Bail Profile fitting of powder diffraction pattern of the1D film.

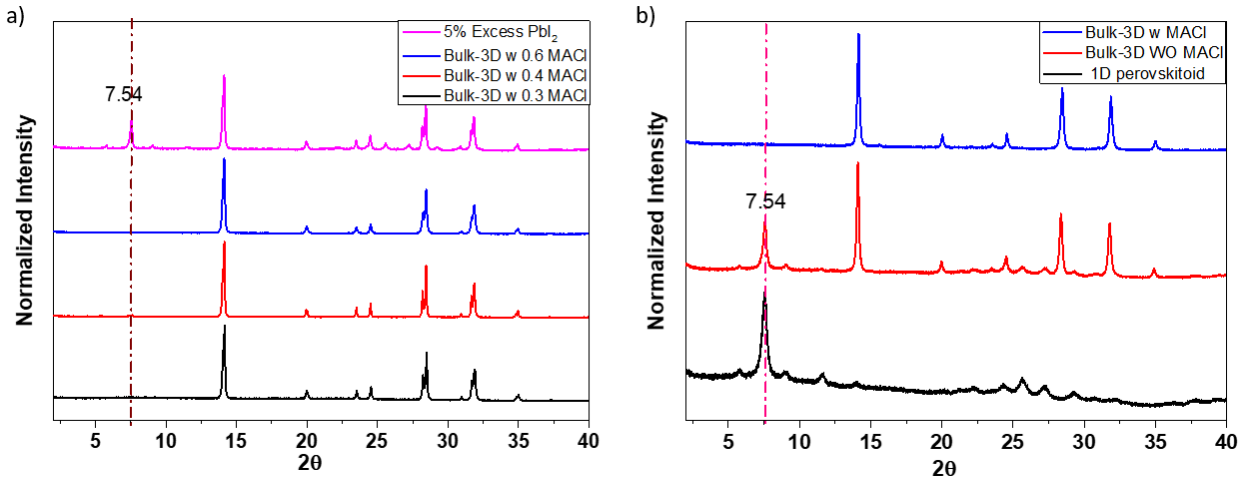

Figure S7. a) Powder XRD patterns of bulk-passivated 3D MAPI with different amount of MACl added (MACl/MAI wt. ratio) b) XRD patterns of 1D and bulk-passivated 3D perovskite with MACI (MACl/MAI (0.5 wt. ratio) and without MACI

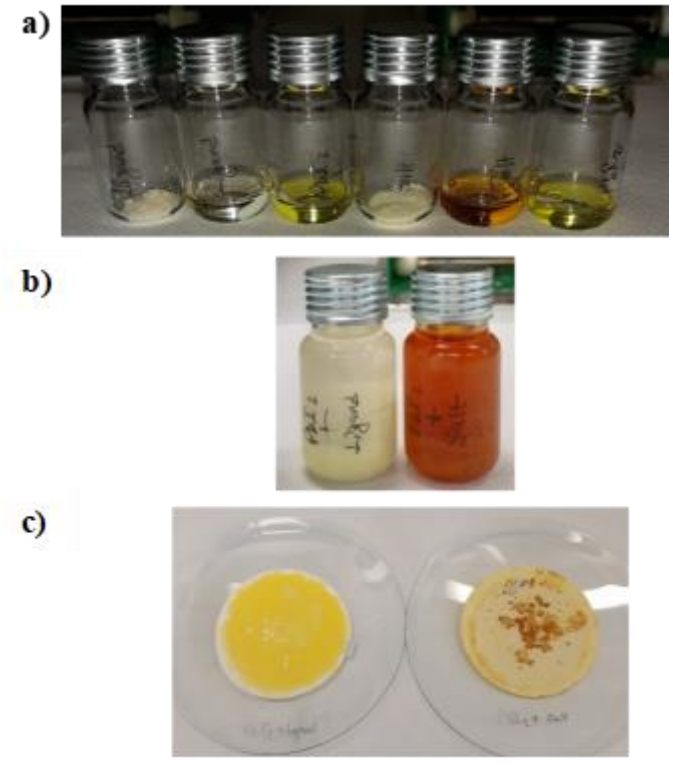

Figure S8. Left to right: a) Photos of the ThPy ligand (unprotonated form of the organic salt) in its pure (solid) form, its solution form in DMF, and its mixture with PbI_2 in DMF; photos of the ThPyI (organic salt) in its pure (solid) form, its solution form in DMF, and its mixture with PbI_2 in DMF. b) Photos of the mixtures of PbI_2 + ThPy, and PbI_2 + ThPyI in DMF with a large amount of toluene, which was stirred at

room temperature for 1 hour. c) Photos of the PbI_2 + ThPy, and PbI_2 + ThPyI precipitates in powder forms which were many times washed with toluene and isopropanol to remove unreacted ligand and its salt form, respectively, dried under vacuum at room temperature for 24 hours.

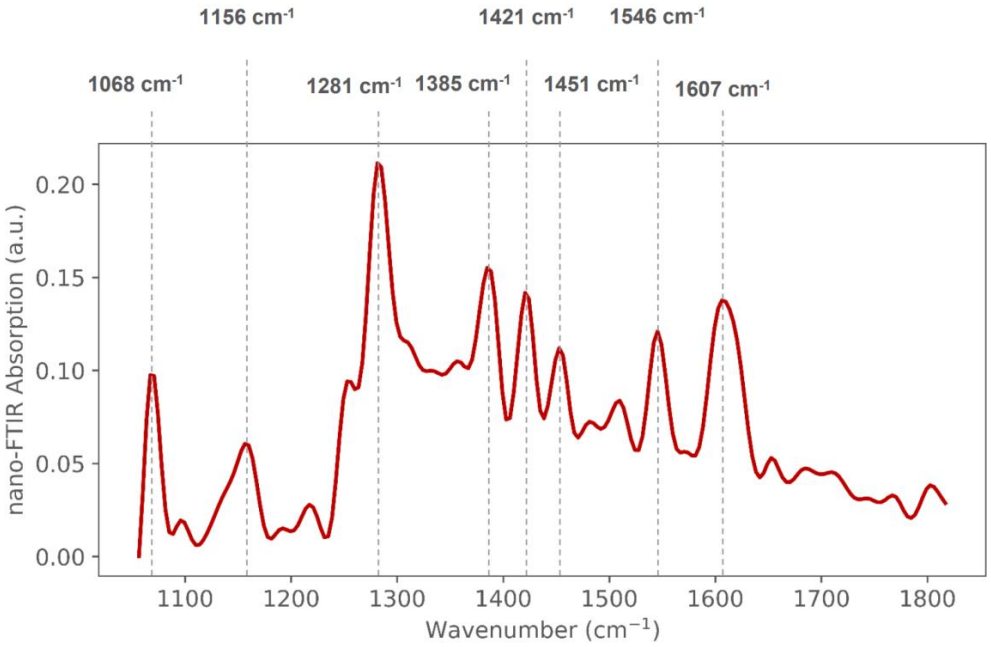

Figure S9. Nano-FTIR Spectra of pure ThPyI.

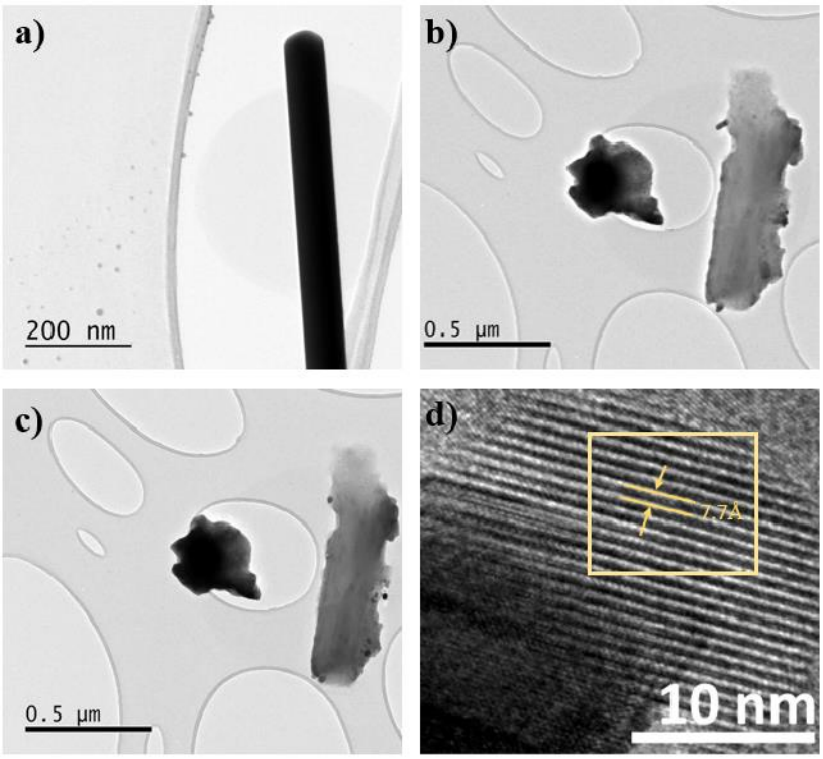

Figure S10. TEM images of bulk-passivated 3D (with MACI) perovskite film.

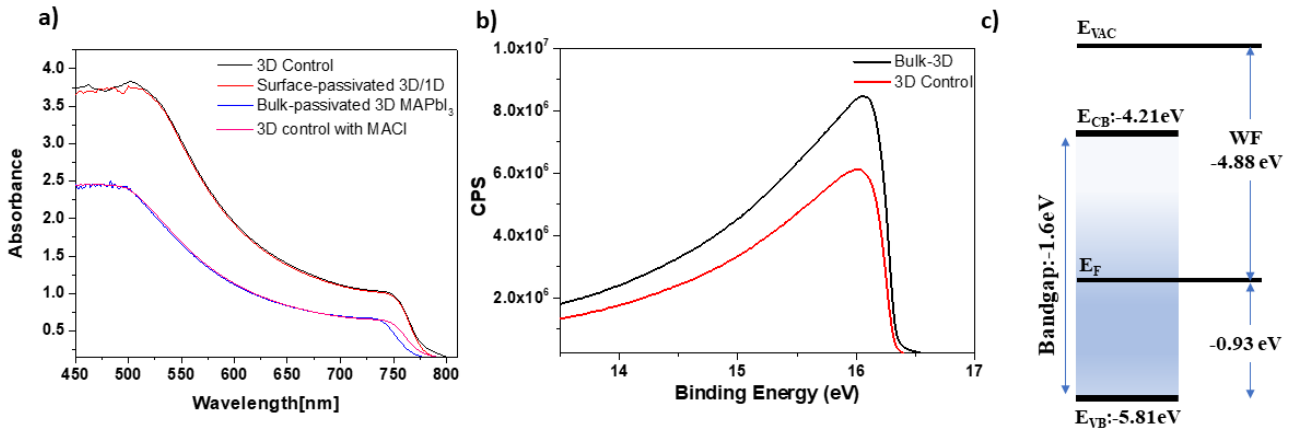

Figure S11. Absorption spectra of 3D MAPI control, surface-passivated 3D/1D and bulk-passivated 3D MAPI. b) Helium Iα ($h\nu$ = 21.22 eV) spectra of SE (secondary electron) cutoff of bulk-passivated 3D perovskite films. c) Schematic energy level diagrams of bulk-passivated 3D perovskite film.

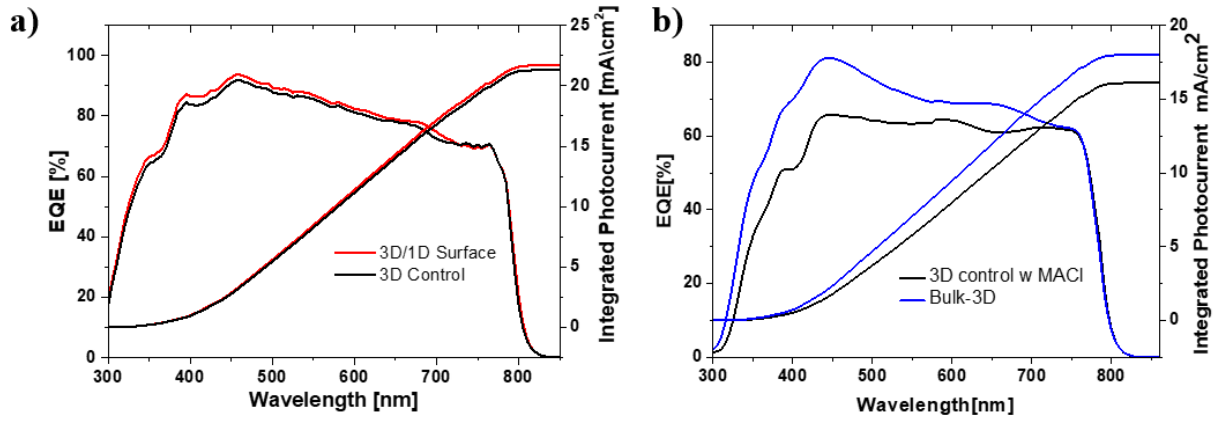

Figure S12. a) EQE of 3D MAPI Control and 3D/1D surface passivated device, b) EQE of 3D MAPI control with MACl and bulk-passivated 3D perovskite.

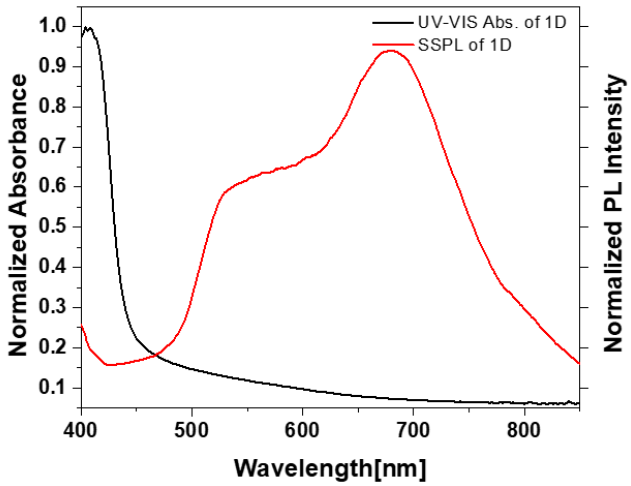

Figure S13. Absorption spectra and SSPL spectra of the1D perovskitoid.

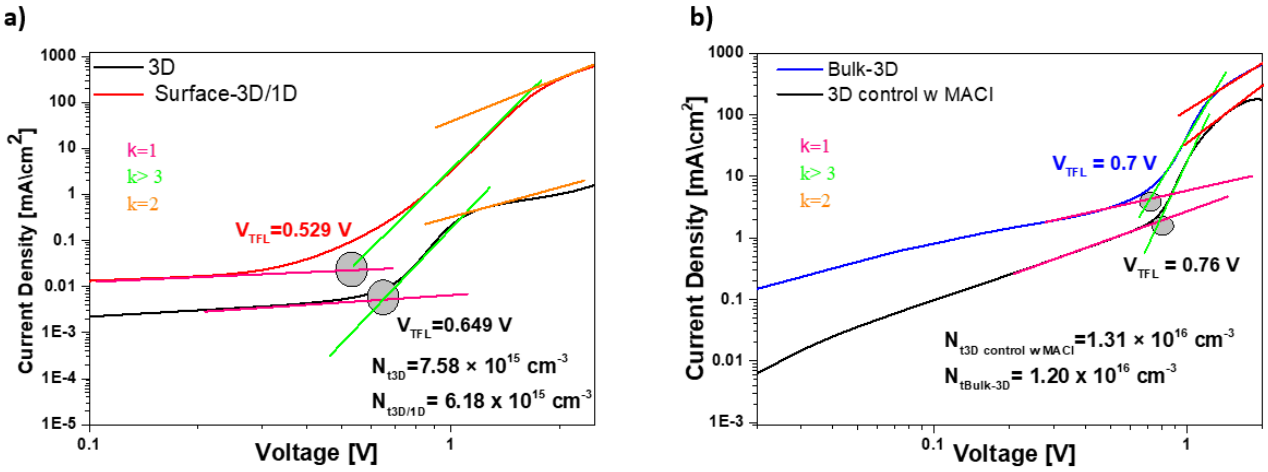

Figure S14. a-b) Electron only devices of the 3D MAPI control, surface-passivated 3D/1D, 3D MAPI control with MACl, and bulk-passivated 3D.

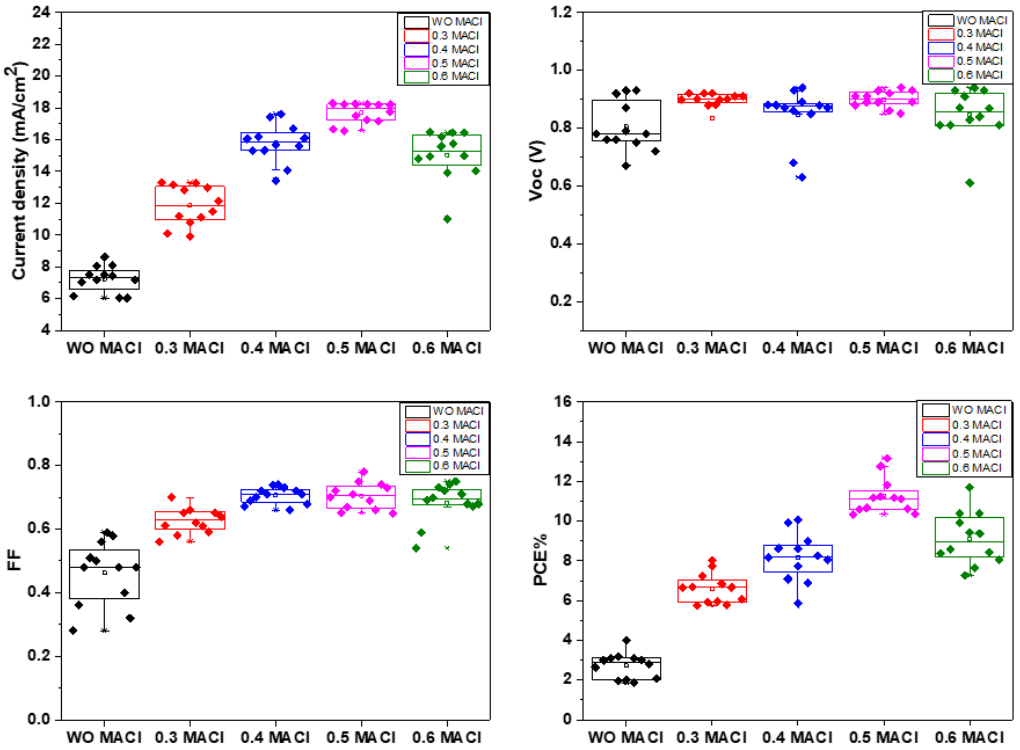

Figure S15. The statistical distribution of photovoltaic parameters of the bulk-3D MAPI with different ratios of MACl in the presence of ThPyI (for example 0.3 MACl means MACl/MAI: 0.3 wt. ratio).

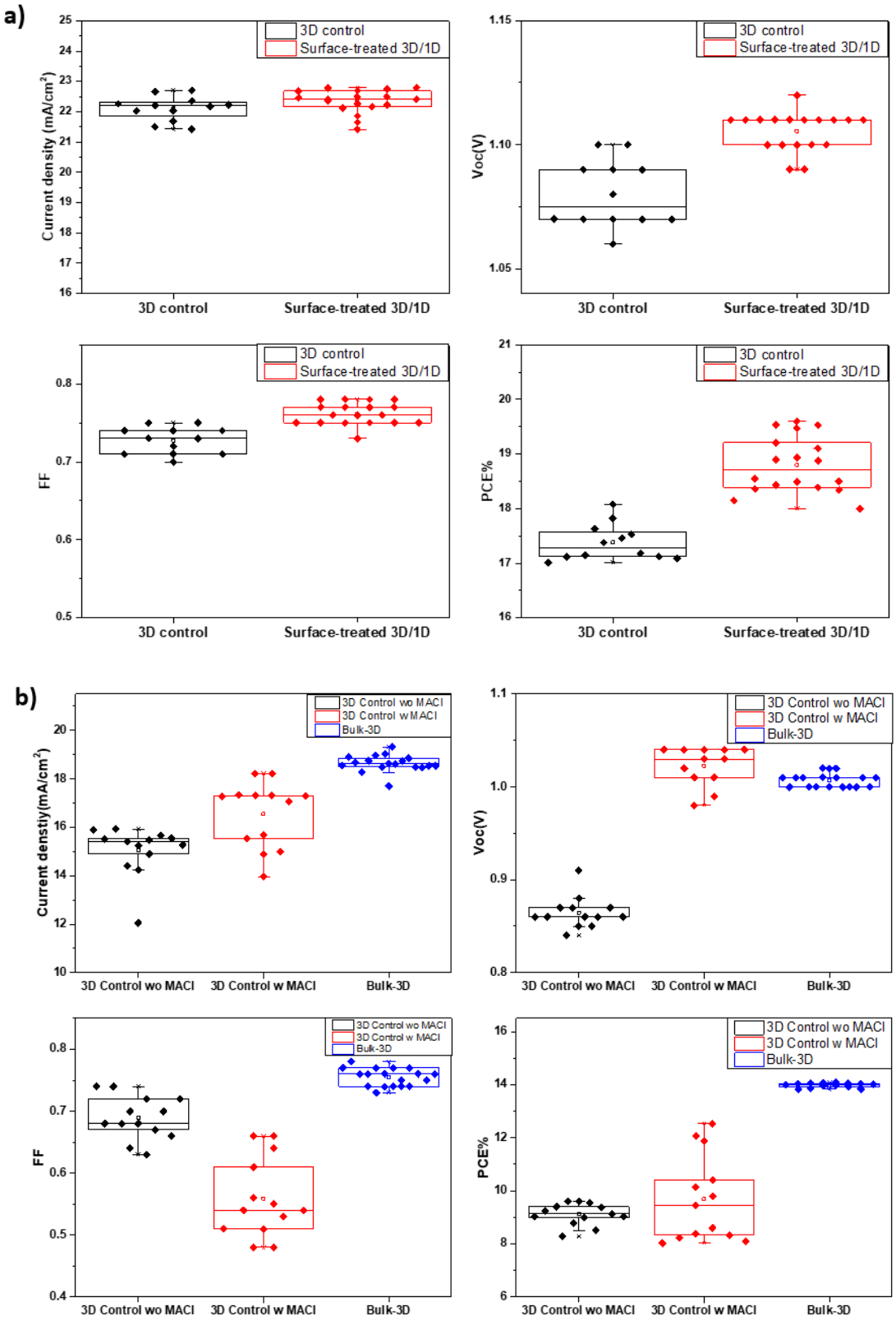

Figure S16. The statistical distribution of photovoltaic parameters of a) Surface-passivated and b) Bulk passivated devices

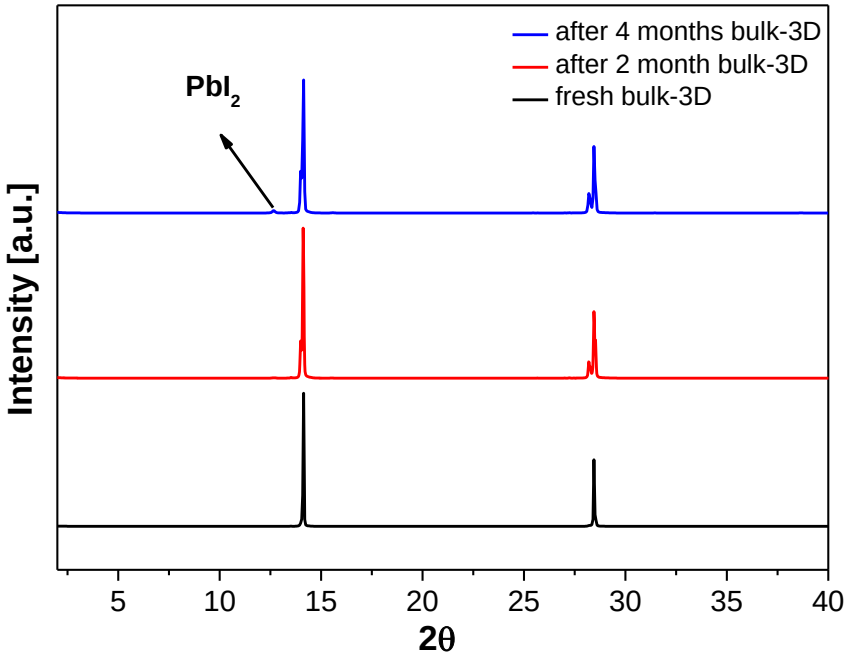

Figure S17. XRD patterns of bulk-passivated 3D perovskite thin films in air after 2 and 4 months.

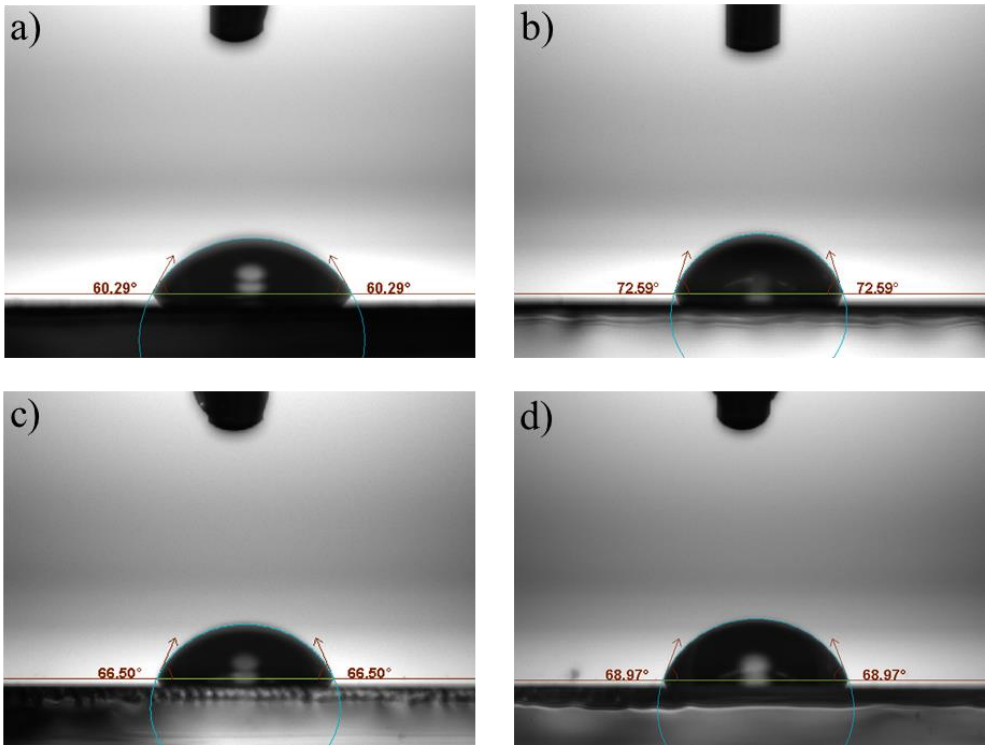

Figure S18. Contact angle measurements of a) 3D $MAPbI_3$ control, b) 1D perovskitoid, c) surface-passivated 3D/1D, and d) bulk-passivated 3D perovskite film.

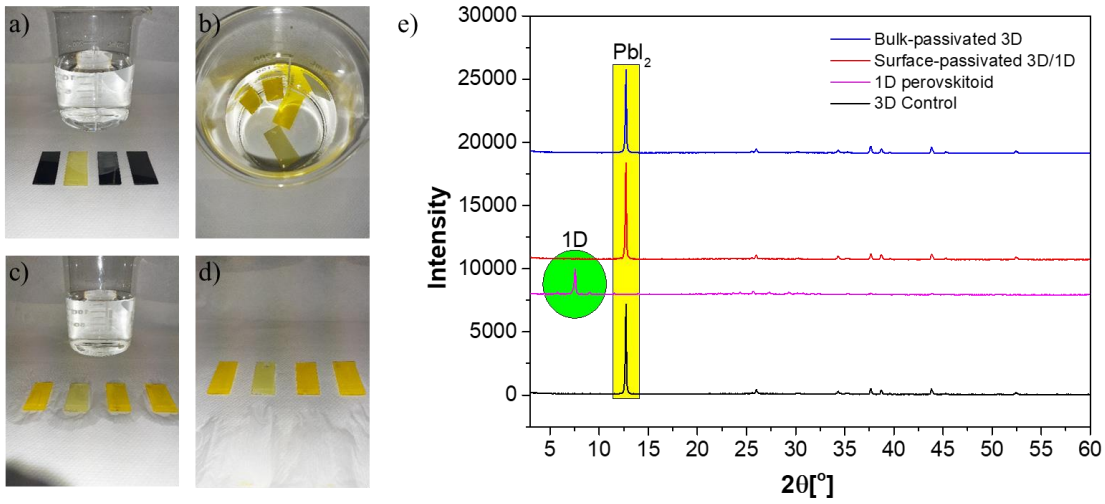

Figure S19. Photos of films, from left to right: a) 3D control, 1D, surface-passivated 3D/1D and bulk-passivated 3D, before water immersion, b) in water, c) after immersion (c), d) after drying, and e) XRD measurements.

Table S1. Crystallographic data of the 1D single crystal

net formula	$C_{18}H_{16}I_8N_2Pb_3S_2$
*M*r/g mol-1	1961.22
crystal size/mm	0.140 × 0.020 × 0.020
T/K	297.(2)
radiation	MoKα
diffractometer	'Bruker D8 Venture TXS'
crystal system	orthorhombic
space group	'F d d 2'
a/Å	25.389(3)
b/Å	61.606(6)
c/Å	4.5767(5)
α/°	90
β/°	90
γ/°	90
V/Å3	7158.5(13)

Z	8
calc. density/g cm-3	3.639
μ/mm-1	21.106
absorption correction	Multi-Scan
transmission factor range	0.33–0.68
refls. measured	24469
*R*int	0.0577
mean σ(*I*)/*I*	0.0488
θ range	3.094–28.281
observed refls.	3993
x, *y* (weighting scheme)	0.0099, 1443.4072
hydrogen refinement	constr
Flack parameter	0.126(18)
refls in refinement	4361
parameters	117
restraints	16
R(*F*obs)	0.0620
*R*w(*F*2)	0.1383
S	1.144
shift/errormax	0.001
max electron density/e Å-3	2.351
min electron density/e Å-3	-3.356

Table S2. Refined structural parameters of the 3D-Control sample.

Refinement was performed using Topas V4.2 SG- I4cm.[5]

Unit cell parameters

a (Å) 8.8706(15)

c (Å) 12.6404(23)

Site	Np	x	y	z	Atom	Occ	Beq
C1	4	0.50000	0.00000	0.61000	C	1	9.475
H1c1	16	0.41950	0.06230	0.58460	H	0.25	11.08
H1n1	16	0.46420	0.91500	0.75200	H	0.25	11.08
H2c1	16	0.59420	0.03860	0.58460	H	0.25	11.08
H2n1	16	0.59150	0.01150	0.75200	H	0.25	11.08
H3c1	16	0.48630	0.89910	0.58460	H	0.25	11.08
H3n1	16	0.44420	0.07350	0.75200	H	0.25	11.08
I1	4	0.00000	0.00000	0.1214(58)	I	1	9.8(3)
I2	8	0.72360(27)	0.22360(27)	0.3590(53)	I	1	6.57(1)
N1	4	0.50000	0.00000	0.72900	N	1	9.475
Pb1	4	0.00000	0.00000	0.3727(51)	Pb	1	3.41(8)

Table S3. a) Part of the Calculated Powder Diffraction Pattern for CuKa1 radiation of the ThPyI based 1D crystal structure data obtained from single crystal

h	**k**	**l**	**d (Å)**	**F(real)**	**F(imag)**	**|F|**	**2θ**	**I**	**M**	**ID(λ)**	**Phase**
0	4	0	15.4015	331.564	59.7401	336.903	5.73363	2.23302	2	1	1
2	2	0	11.737	2072.66	303.527	2094.77	7.52601	100	4	1	1
2	4	0	9.79595	-751.68	-114.89	760.41	9.02013	9.15337	4	1	1
2	6	0	7.98325	-251.85	-77.194	263.416	11.0741	0.72611	4	1	1
0	8	0	7.70074	-767.67	-66.537	770.553	11.4817	2.88768	2	1	1
2	8	0	6.58405	209.808	42.3422	214.038	13.4373	0.32396	4	1	1
4	0	0	6.34735	954.273	47.4506	955.452	13.9409	2.99516	2	1	1
4	2	0	6.21674	-399.51	-9.8048	399.634	14.2353	1.00437	4	1	1
4	4	0	5.86851	478.925	61.4956	482.857	15.0847	1.30293	4	1	1
2	10	0	5.54243	242.154	47.2985	246.73	15.9779	0.3025	4	1	1

Table S4. The interplanar lattice distances of some planes

h	k	l	d (Å)
2	2	0	11.74
0	8	0	7.70
2	3	1	2.87

Table S5. Time-resolved photoluminescence decay components of MAPI reference, surface, and bulk-treated MAPI films.

Sample	A_1(%)	τ_1 (µs)	A_2 (%)	τ_2 (µs)	$\tau_{ave.}$ (µs)
3D MAPI Control	58.19	0.050	41.81	0.114	0.076
Surface passivated 3D/1D	38.14	0.068	61.86	0.214	0.158
Bulk-passivated 3D	36.06	0.055	63.94	0.154	0.118
3D control with MACl	50.12	0.049	49.88	0.087	0.068

Table S6. Photovoltaic Parameters for the champion devices (reverse scan values are reported in parentheses)

Device	Jsc (mA\cm^2)	PCE %	Voc (V)	FF	Integrated Photocurrent (mA\cm^2)	Hysteresis Index %
3D Control	22.35(22.17)	18.08(17.01)	1.09(1.07)	0.74(0.72)	21.305 (Jsc -4,7%)	5.92
3D/1D Surface	22.69(22.79)	19.60(19.53)	1.11(1.10)	0.78(0.78)	21.692 (Jsc -4,4%)	0.35
3D control with MACl	17.81(16.54)	12.53(9.68)	1.03(1.02)	0.66(0.55)	16.09 (Jsc-9.6%)	16.9
Bul- 3D MAPI	18.98(18.94)	13(14.10)	1.02(1.01)	0.72(0.74)	18.00 (Jsc-5.11 %)	2.55

REFERENCES

[1] APEX, Bruker, and Bruker AXS SAINT. Inc.: Madison, Wisconsin, USA, **2012**
[2] G. M. Sheldrick, *SADABS, Empirical Absorption Correction Program*, University of Göttingen, Germany,**1997**.
[3] Sheldrick, G. M. *Acta Cryst.*, **2015**. *A71*, 3.
[4] Farrugia, L. J. J. *Appl. Cryst*., **2012**. *45*, 849.
[5] TOPAS V4.2, General Profile and Structure Analysis Software for Powder Diffraction Data. In Tutorial; Bruker AXS: Karlsruhe, Germany, 2009.